

Comparison of diagnostic efficacy of MRI and PET/CT in lung cancer of mouse with spinal metastasis

Wenkai Hu¹, Zheng Liu¹, Xiao Xiao¹, Yan Yang¹, Zhicheng Sun¹, Xiyang Wang^{1,2*}¹ Department of Spine Surgery, Xiangya Hospital, Central South University, Changsha 410008, China² Hunan Engineering Laboratory of Advanced Artificial Osteo-Materials, Xiangya Hospital, Central South University, Changsha 410008, China

*Correspondence to: wvf3a4@163.com

Received February 14, 2020; Accepted May 17, 2020; Published June 5, 2020

Doi: <http://dx.doi.org/10.14715/cmb/2020.66.3.21>

Copyright: © 2020 by the C.M.B. Association. All rights reserved.

Abstract: This study aimed to compare the diagnostic efficacy of MRI and PET/CT in lung cancer of mouse with spinal metastasis. 40 healthy Balb/c nude mice were selected. 0.1 ml of human lung cancer cell A549 bacterial suspension was injected by the left ventricle injection method to establish a lung cancer spinal metastasis model, and the abnormal signs of the nude mice were closely observed. When the body weight was reduced by 20%, micro PET/CT imaging and small coil MRI imaging were applied after intraperitoneal injection of thiopental anesthesia in nude mice. After the imaging was completed, the nude mouse was dissected and the spinal tumor was removed. The nature of spinal metastases was diagnosed by the pathology department. 5 nude mice died of abdominal infection, 2 nude mice had no spinal tumors, and the remaining 33 nude mice were successfully modeled. 33 nude mice were confirmed by pathology to have 64 metastatic vertebral lesions, among them, there were 7 cervical vertebrae, 24 thoracic vertebrae, 16 lumbar vertebrae, 6 sacral vertebrae and 11 caudal vertebrae. The sensitivity of MRI in the diagnosis of spinal metastases was 78.13%, and specificity was 56.25%. The sensitivity of PET/CT for the diagnosis of spinal metastases was 92.19%, and specificity was 78.95%. The specificity and positive predictive value of PET/CT for the diagnosis of spinal metastases were not significantly different from those of MRI ($P > 0.05$). The sensitivity, accuracy and negative predictive values were significantly higher than those of MRI ($P < 0.05$). PET/CT is superior to MRI in the diagnosis of spinal metastases, and its sensitivity, accuracy and negative predictive values were significantly higher than those of MRI ($P < 0.05$). It is worthy to be further promoted in clinical practice.

Key words: MRI; PET/CT; Lung adenocarcinoma; Spinal metastases; The diagnostic value.

Introduction

Lung cancer is the most common cancer globally (1). Its morbidity and mortality are high, and the incidence of lung cancer is still growing (2, 3). Lung cancer is often manifested as metastatic disease, with a special tendency to metastasize to bones (4, 5). Bone metastasis is a common metastasis site in patients with lung cancer. Lung cancer bone metastasis not only has a serious impact on the quality of life of patients but also has a poor prognosis (6). These metastases are associated with significant morbidity, loss of functional independence, and decreased quality of life (7). A large number of patients with cancer died each year due to bone metastases (8), and spinal metastasis is the most common site of lung cancer bone metastasis, accounting for about 50% of patients with lung cancer bone metastasis (9).

The PET/CT integrated imaging system is a dual-mode imaging system that combines both positron emission tomography (PET) and CT in a single device (10, 11). PET/CT diagnosis enables oncologists to view images within the anatomical framework provided by CT, which has better visualization and appreciation for the molecular information provided by PET. However, 18F-FDG can be used as a "contrast agent" for radiologists. This is because 18F-FDG can highlight anatomi-

cally under-recognized but suggestive lesions (12). Magnetic resonance imaging (MRI), due to its good soft-tissue resolution, is the preferred imaging method for assessing intramedullary cavity metastasis, tumor expansion from the medullary cavity, and surrounding structural involvement (13). What's more, MRI is very sensitive to the detection of bone metastases. This is due to the ability to display a focal aggregation map of radiotracers on bone scans before cortical destruction occurs (14, 15).

Currently, the diagnosis of lung cancer spinal metastases is depending on CT, MRI and other imaging studies, only a few PET/CT were used. This study aimed to establish a nude mouse model of lung cancer spinal metastasis, using PET/CT, MRI for diagnosis, also pathological results were compared to determine its diagnostic value.

Materials and Methods

Lung cancer cell lines

10% of inactivated fetal bovine serum was used in the DMEM medium (Shanghai Xinyu Biotechnology Co. Ltd., Item No.: 19-0040-100). Human lung cancer cell A549 was cultured (Shanghai Enzyme Research Biotechnology Co. Ltd. article number: ATCC-76). The cells were digested and passaged with 0.25% of trypsin

(Shanghai Beinuo Biotechnology Co. Ltd., Item No.: T4049-500ML). Centrifuge at 1500 rpm for 5 min at standard room temperature. Discarding the supernatant and washing it with PBS (Shanghai Lianmai Bioengineering Co. Ltd., item number: LM0221A), after centrifugation at 800 rpm for 8 min, the cells were diluted with PBS to prepare for a suspension with a concentration of $1 \times 10^7/\text{mL}$.

Research objects and modeling

40 healthy Balb/c nude mice were selected, all of them were males, aged between 8-10 weeks, weighted between 18-21g, were purchased from Changzhou Cavans Experimental Animal Co. Ltd, and the animal certificate number is SCXK (Su) 2011-0003. They were kept in a room with no special pathogens at a room temperature of 23 – 25 °C and humidity of 55-62%, and were free to drink water. All mice were modeled after 1 week of adaptive feeding.

Nude mice were injected intraperitoneally with pentobarbital sodium 60 mg/kg for anesthesia (Shanghai Xinya Pharmaceutical Co. Ltd., SFDA approval number: H31021724). Disinfect the skin with 75% alcohol (Shanghai Youyu Biotechnology Co., Ltd., item number: YYJK-916), the limbs were fixed on the bench. A small incision of 2-3 cm was drawn from the left side of the second intercostal line of the nude mouse. The needle was tilted from the inside down and was injected obliquely upward. It was at an angle of 45° to the horizontal and vertical axes of the nude mouse. Gently remove the needle when it was inserted approximately 5-6 mm. If there was bright red blood in the syringe, it indicated the left ventricle was successfully punctured. At this point, keep the empty needle stable, and then slowly inject 0.1mL of the cell suspension into the left ventricle. After the cell suspension was fully injected, re-extract to confirm whether there was red blood in the syringe. After a successful injection, the cotton ball was used to gently press the pinhole. Finally, wait for the nude mouse to regain consciousness and monitor their vital signs. The left ventricle was injected with the cell suspension for 2 weeks, and the nude mice were weighed daily and the abnormal signs were closely observed. Being unable to eat or drink, uncontrolled bleeding, severe respiratory infection, and abnormal central nervous response were considered humane endpoints (16), and animals exhibiting signs of such endpoints received a large dose of the anesthetic drug in the abdominal cavity. Death was confirmed when no physiological response was observed and no vital signs were detected.

Animal imaging test

After the inoculation of lung cancer cell, A549 from the left ventricle (17), severe systemic failure, shortness of breath and a 20% weight loss in nude mice indicate that the mice have had cachexia. Nude mice were injected intraperitoneally with 50mg/kg of 1% thiopental sodium for nude mice (18) (Shanghai Xiyuan Biotechnology Co. Ltd., article number: XY-EP-T1200000). After anesthesia, apply inveon micro PET/CT imaging (Siemens Preclinical Solution, Knoxville, TN, USA), and 1.5 Tesla MRI unit small coil MRI imaging (Philips Healthcare, The Netherlands).

Micro PET/CT scanners imaging: The mice fasted

for more than 6 h before PET/CT test; after anesthesia, the modeled nude mice were injected with 18F-FDG (purchased from Hefei Bomei Biotechnology Co. Ltd.). The dose was 0.2mci/unit, and micro CT and micro PET were performed half an hour later. In the meanwhile, the number of lesions in the spine was recorded.

Collection of MRI with sense body

MRI imaging in mice does not require the injection of contrast agents. Then apply for a T-weighted image axial position, sagittal scanning (TR 500 MHz, TE 20 MHz) and T-weighted fat-filled axial position, coronal scanning (TR 4360 M Hz, TE 114M Hz), respectively. The back spine of the nude mice was scanned, and the suspected bone lesions were scanned by STIR sequence, and some cases were scanned by enhanced scanning, with a layer thickness of 4 mm and an interval of 1 mm. In the meanwhile, the number of lesions in the spine was recorded.

Pathological test

After the imaging was completed, the nude mice were sacrificed by cervical dislocation and dissected, and the spinal tumors were removed and labeled separately. The lesion tissue was routinely dehydrated, immersed, embedded, and serially sliced with 10% of formaldehyde. The sections were 4µm in thickness and were observed after HE staining. The nature of spinal metastases was diagnosed by pathology.

Imaging Analysis

Image analysis was performed by two experienced imaging physicians combined with the pathological test to confirm the diagnosis of spinal metastases. The diagnostic efficacy of both imaging methods was compared with the pathological test, and the sensitivity, specificity, accuracy, positive predictive value and negative predictive value were used as evaluation indicators.

Statistical analysis

The analysis was performed using SPSS 20.0 statistical software (Shanghai Kabe Information Technology Co. Ltd.). The count data were used by the χ^2 test. Comparisons at different times within the group were analyzed by repeated measures of ANOVA, and the Bonferroni test was the post hoc test. $P < 0.05$ was considered statistically significant.

Results

Nude mouse weight data

The bodyweight of nude mice gradually decreased during week 2 to week 6 of modeling, and the difference was statistically significant ($P < 0.001$). The weight of nude mice was not significantly different between week 3 and week 2 of modeling with week 5 and week 6 of modeling ($P > 0.05$). Models of the weight of nude mice at week 4, 5 and 6 were significantly less than those at week 2; models of the weight of nude mice at week 5 and 6 were significantly less than those at week 3; models of the weight of nude mice at week 6 were significantly less than week 5, and the difference was statistically significant ($P < 0.05$). The maximum percentage of body weight loss due to cachexia was 24.61% (Table 1 and

Table 1. Changes in body weight of 33 nude mice during modeling.

Modeling time	Weight (g)
2 weeks	20.11±1.73
3 weeks	19.91±1.01
4 weeks	18.24±1.97ab
5 weeks	17.03±1.84abc
6 weeks	16.27±1.77abc
F	33.21
P	0.001

Figure 1).

The bodyweight of nude mice gradually decreased during week 2 to week 6 of modeling, and the difference was statistically significant ($P < 0.001$). The weight of nude mice was not significantly different between week 3 and week 2 of modeling with week 5 and week 6 of modeling ($P > 0.05$). Models of the weight of nude mice at week 4, 5 and 6 were significantly less than those at week 2; models of the weight of nude mice at week 5 and 6 were significantly less than those at week 3; models of the weight of nude mice at week 6 were significantly less than week 4, and the difference was statistically significant ($P < 0.05$).

Modeling Results

The results have shown that 5 nude mice died within 4 weeks after modeling, and the mortality rate was 12.5% (19). After anatomy, it was assumed that the cause of death was an abdominal infection, 2 nude mice had no spinal tumors; after the remaining 33 nude mice were molded for 5 weeks, the nude mice showed signs of reduced eating, lethargy, and slow movement. Some nude mice had prominent back, abdomen or tail, indicating successful modeling, with a modeling success rate of 82.5%. 33 nude mice were confirmed by pathology to have 64 metastatic vertebral lesions, among them, there were 7 cervical vertebrae, 24 thoracic vertebrae, 16 lumbar vertebrae, 6 sacral vertebrae and 11 caudal vertebrae.

Comparison of Diagnostic Value

33 lung adenocarcinoma nude mice were found to have 80 lesions by MRI, among them, 64 cases were confirmed to be metastatic vertebral lesions by pathology and 16 cases were benign lesions. Sensitivity 50/64, which was 78.13%, specificity 9/16, 56.25%, accuracy (50+9)/80, which was 73.75%; the positive

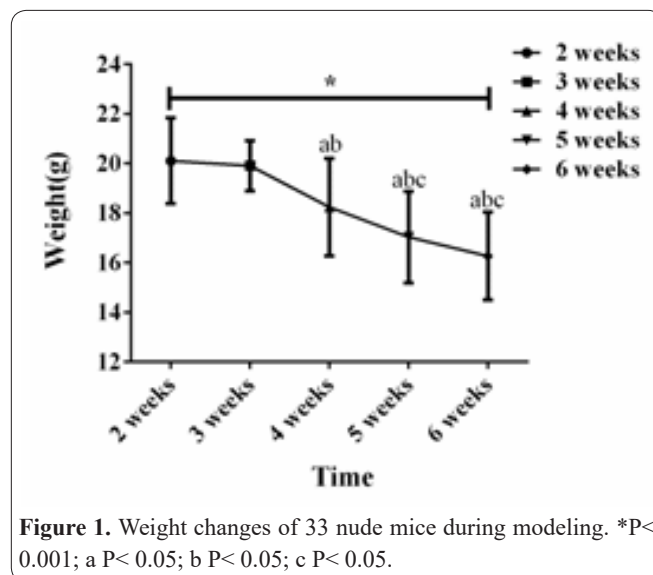


Figure 1. Weight changes of 33 nude mice during modeling. * $P < 0.001$; a $P < 0.05$; b $P < 0.05$; c $P < 0.05$.

predictive value was 50/57, which was 87.72%; the negative predictive value was 9/23, which was 39.13%. 33 lung adenocarcinoma nude mice were found to have 83 lesions by PET/CT, among them, 64 cases were confirmed to be metastatic vertebral lesions by pathology and 19 cases were benign lesions. Sensitivity 59/64, which was 92.19%; specificity 15/19, which was 78.95%; accuracy (59+15)/83, which was 89.16%; the positive predictive value, was 59/63, which was 93.65%; the negative predictive value was 15/20, which was 75.00% (Table 2).

The specificity and positive predictive value of PET/CT for the diagnosis of spinal metastases were not significantly different from MRI ($P > 0.05$). Sensitivity, accuracy, and negative predictive value were significantly higher than MRI, and the difference was statistically significant ($P < 0.05$).

Discussion

Left ventricular injection, used in this study to establish a nude mouse model of spinal metastases, is widely used in the clinical practice. Arguello *et al.* (20) first reported the successful experience of using left ventricular injection to make bone metastasis models in nude mice, which has the characteristics of strong reproducibility and high success rate. It is currently believed that metastasis of malignant tumors is transferred to the spine through the bloodstream. The transarterial

Table 2. Comparison of the diagnostic efficacy of MRI and PET/CT in spinal metastases.

	MRI	PET/CT	X ²	p
TP	50	59		
FP	7	4		
FN	14	5		
TN	9	15		
Sensitivity	78.13	92.19	5.006	0.045
Specificity	63.16	78.95	2.076	0.273
Accuracy	74.70	89.16	6.439	0.015
95% confidence interval	1.451~14.529	10.571~185.228	-	-
Positive predictive value	87.72	46.15	1.264	5.581
Negative predictive value	93.65	75.00	0.347	0.031

routes of metastases formation are metastasis of thyroid cancer, liver cancer, lung cancer and other malignant tumors to the spines (21, 22). In this study, we aimed to establish the lung metastasis model of lung cancer stem cells in nude mice based on lung cancer cell lines. This is for further study on the diagnostic value of MRI and PET/CT in spinal metastasis of lung adenocarcinoma in nude mice.

The results of this study showed that the sensitivity of MRI in the diagnosis of spinal metastases was 78.13%; specificity was 56.25%; accuracy was 73.75%; the positive predictive value was 87.72%, and the negative predictive value was 39.13%. The sensitivity of PET/CT for the diagnosis of spinal metastases was 92.19%; specificity was 78.95%; accuracy was 89.16%; the positive predictive value was 93.65%, and the negative predictive value was 75.00%. The specificity and positive predictive value of PET/CT for the diagnosis of spinal metastases were not significantly different from MRI ($P > 0.05$). The sensitivity, accuracy and negative predictive values were significantly higher than those of MRI, and the difference was statistically significant ($P < 0.05$). Therefore, PET/CT is superior to MRI in the diagnosis of spinal metastases in nude mice. Qu *et al* (23) conducted a meta-analysis of lung cancer patients and 18F-FDG PET/CT and MRI were used to assess the ability of bone metastases from lung cancer. The results showed that 18F-FDG PET/CT was a better imaging method for diagnosing bone metastasis than MRI because 18F-FDG PET/CT has higher diagnostic values (sensitivity, specificity). This is consistent with the results of our study because 18F-FDG PET/CT can directly detect the presence of tumors through metabolic activities, rather than indirectly detecting the presence of tumors by increasing the conversion of bone minerals, which resulted in a higher level of accuracy. In the past few decades, PET can provide functional data using the glucose analog 18F-FDG. It has risen from the initial research tool to the basic imaging tool for assessing lung cancer (24-36).

In addition, with the development of technology, FDG-PET imaging and CT fusion has become a new model for a variety of oncology imaging (PET/CT) (37, 38). The advantage of PET/CT over traditional MRI is that it can detect changes in metabolism before structural changes occur in the lesion tissues, whereas, MRI can only detect changes in the structure of the disease after structural changes in the tissue (39). Priority uptake of 18F-FDG in tumor cells produces a high tumor-background intensity ratio; this contributes to the detection of tumor lesions and the study of tumor cell characteristics (40). In MRI imaging, bone metastases usually appear as discrete foci of low T1 signals, corresponding to the replacement of normal fat marrow by malignant cells. In the T2-weighted sequence, bone metastases usually appear as T2 high intensity. This is due to its increased water content, and sputum enhancement is due to increased blood vessels (41, 42). However, the sensitivity of MRI to bone destruction is much lower than its sensitivity to intramedullary lesions. Whereas, PET/CT can perform images of soft tissues, and observe bone tissues and provide the specific anatomical location of metastases (43, 44). Clinical trials will be conducted in the future to justify the conclusions of this study. In

summary, PET/CT is superior to MRI in the diagnosis of spinal metastases. Its sensitivity, accuracy and negative predictive value are significantly higher than MRI. It is worthy to be further promoted in clinical practice.

Funding

This study was supported by clinical scientific research funds of Xiangya Hospital (No. 2016L07) and the National Natural Science Foundation of China (No.81672191).

Competing interests

The authors declare that they have no competing interests.

References

1. Eguchi T, Bains S, Lee MC, Tan KS, Hristov B, Buitrago DH, Bains MS, Downey RJ, Huang J, Isbell JM, Park BJ, Rusch VW, Jones DR, Adusumilli PS. Impact of Increasing Age on Cause-Specific Mortality and Morbidity in Patients with Stage I Non-Small Cell Lung Cancer: A Competing Risks Analysis. *J Clin Oncol* 2016; 35: 281-290.
2. Park JS, Bateni SB, Bold RJ, Kirane AR, Canter DJ, Canter RJ. The modified frailty index to predict morbidity and mortality for retroperitoneal sarcoma resections. *J Surg Res* 2017; 217: 191-197.
3. Al Husaini H, Wheatley-Price P, Clemons M, Shepherd FA. Prevention and management of bone metastases in lung cancer: a review. *J Thorac Oncol* 2009; 4: 251-259.
4. Zaritsky A. Challenges and Technological Trends Toward Improved Medical Imaging-based Predictive Data-mining. *EBioMedicine* 2018; 35: 20-21.
5. Coleman RE. Metastatic bone disease: clinical features, pathophysiology and treatment strategies. *Cancer Treat Rev* 2001; 27: 165-176.
6. Berenson J, Rajdev L, Broder M. Managing bone complications of solid tumors. *Cancer Biol Ther* 2006; 5: 1086-1089.
7. Ortiz GJ, Lozano G. SNPing away at mutant p53 activities. *Genes Dev* 2018; 32: 195-196.
8. Tsuya A, Kurata T, Tamura K, Fukuoka M. Skeletal metastases in non-small cell lung cancer: a retrospective study. *Lung Cancer* 2007; 57: 229-232.
9. Beyer T, Townsend DW, Brun T, Kinahan PE, Charron M, Roddy R, Jerin J, Young J, Byars L, Nutt R. A combined PET/CT scanner for clinical oncology. *J Nucl Med* 2000; 41: 1369-1379.
10. Czernin J, Allen-Auerbach M, Schelbert HR. Improvements in cancer staging with PET/CT: literature-based evidence as of September 2006. *J Nucl Med* 2007; 48: 78S-88S.
11. Spick C, Herrmann K, Czernin J. 18F-FDG PET/CT and PET/MRI perform equally well in cancer: evidence from studies on more than 2,300 patients. *J Nucl Med* 2016; 57: 420-430.
12. Costelloe CM, Rohren EM, Madewell JE, Hamaoka T, Theriault RL, Yu TK, Lewis VO, Ma J, Stafford RJ, Tari AM, Hortobagyi GN, Ueno NT. Imaging bone metastases in breast cancer: techniques and recommendations for diagnosis. *Ancol Oncol* 2009; 10: 606-614.
13. Bäuerle T, Semmler W. Imaging response to systemic therapy for bone metastases. *Eur Radiol* 2009; 19: 2495-2507.
14. Rajarubendra N, Bolton D, Lawrentschuk N. Diagnosis of bone metastases in urological malignancies-an update. *Urology* 2010; 76: 782-790.
15. Haley HR, Shen N, Qyli T, Buschhaus JM, Pirone M, Luker KE, Luker GD. Enhanced Bone Metastases in Skeletally Immature Mice. *Tomography* 2018; 4: 84-93.
16. Close B, Banister K, Baumans V. Recommendations for eutha-

nesia of experimental animals: Part 1. *Laboratory Animal* 1996; 30: 293-316.

17. Ye SF, Li J, Ji SM, Zeng HH, Lu W. Dose-biomarker-response modeling of the anticancer effect of ethaselen in a human non-small cell lung cancer xenograft mouse model. *Acta Pharmacologica Sinica* 2017; 38(2): 223-232.

18. Hubbard TF, Goldbaum LR. The mechanism of tolerance to thiopental in mice. *J Pharmacol Exp Ther* 1949; 97: 488-491.

19. Newman, KB. State-Space Modeling of Animal Movement and Mortality with Application to Salmon. *Biometrics* 1998; 1: 1290-1314.

20. Futakuchi M, Singh RK. Animal model for mammary tumor growth in the bone microenvironment. *Breast Cancer* 2013; 20: 195-203.

21. Thudi NK, Martin CK, Nadella MV, Fernandez SA, Werbeck JL, Pinzone JJ, Rosol TJ. Zoledronic acid decreased osteolysis but not bone metastasis in a nude mouse model of canine prostate cancer with mixed bone lesions. *Prostate* 2010; 68: 1116-1125.

22. Menezes ME, Das SK, Minn I, Emdad L, Wang XY, Sarkar D, Pomper MG, Fisher PB. Detecting Tumor Metastases: The Road to Therapy Starts Here. *Adv Cancer Res* 2016; 132: 1-44.

23. Konert T, van-de-Kamer JB, Sonke JJ, Vogel WV. The developing role of FDG PET imaging for prognostication and radiotherapy target volume delineation in non-small cell lung cancer. *J Thorac Dis* 2018; 10: S2508-S2521.

24. Toloza EM, Harpole L, McCrory DC. Noninvasive staging of non-small cell lung cancer*: a review of the current evidence. *Chest* 2003; 123: 137S-146S.

25. Budak E, Çok G, Akgün A. The Contribution of Fluorine 18F-FDG PET/CT to Lung Cancer Diagnosis, Staging and Treatment Planning. *Mol Imaging Radionucl Ther* 2018; 27: 73-80.

26. Nie Y, Luo F, Lin Q. Dietary nutrition and gut microflora: A promising target for treating diseases. *Trends Food Sci Technol* 2018; 75: 72-80.

27. Ren Y, Jiao X, Zhang L. Expression level of fibroblast growth factor 5 (FGF5) in the peripheral blood of primary hypertension and its clinical significance. *Saudi J Biol Sci* 2018; 25(3): 469-473.

28. Guo T, Lin Q, Li X, Nie Y, Wang L, Shi L, Luo F. Octacosanol attenuates inflammation in both RAW264. 7 macrophages and a mouse model of colitis. *J Agri Food Chem* 2017; 65(18): 3647-3658.

29. Li W, Jia MX, Wang JH, Lu JL, Deng J, Tang JX, Liu C. Association of MMP9-1562C/T and MMP13-77A/G polymorphisms with non-small cell lung cancer in southern Chinese population. *Biomol* 2019; 9(3): 107-119.

30. Nie Y, Luo F, Wang L, Yang T, Shi L, Li X, Shen J, Xu W, Guo T, Lin Q. Anti-hyperlipidemic effect of rice bran polysaccharide and its potential mechanism in high-fat diet mice. *Food Func* 2017; 8(11): 4028-4041.

31. Lou Y, Yang J, Wang L, Chen X, Xin X, Liu Y. The clinical efficacy study of treatment to Chiari malformation type I with syringomyelia under the minimally invasive surgery of resection of

Submeningeal cerebellar Tonsillar Herniation and reconstruction of Cisterna magna. *Saudi J Biol Sci* 2019; 26(8): 1927-1931.

32. Lou Y, Guo D, Zhang H, Song L. Effectiveness of mesenchymal stem cells cultured by hanging drop vs. conventional culturing on the repair of hypoxic-ischemic-damaged mouse brains, measured by stemness gene expression. *Open Life Sci* 2016; 11(1): 519-523.

33. Liang Y, Lin Q, Huang P, Wang Y, Li J, Zhang L, Cao J. Rice Bioactive Peptide Binding with TLR4 To Overcome H2O2-Induced Injury in Human Umbilical Vein Endothelial Cells through NF- κ B Signaling. *J Agri Food Chem* 2018; 66(2): 440-448.

34. Wang L, Lin Q, Yang T, Liang Y, Nie Y, Luo Y, Luo F. Oryzanol modifies high fat diet-induced obesity, liver gene expression profile, and inflammation response in mice. *J Agri Food Chem* 2017; 65(38): 8374-8385.

35. Lou Y, Shi J, Guo D, Qureshi AK, Song L. Function of PD-L1 in antitumor immunity of glioma cells. *Saudi J Biol Sci* 2017; 24(4): 803-807.

36. Chen X, Xu Y, Meng L, Chen X, Yuan L, Cai Q, Shi W, Huang G. Non-parametric partial least squares-discriminant analysis model based on sum of ranking difference algorithm for tea grade identification using electronic tongue data identify tea grade using e-tongue data. *Sens Actuators B Chem* 2020; 311: 127924-127931.

37. Cerfolio RJ, Ojha B, Bryant AS, Raghuvveer V, Mountz JM, Bartolucci AA. The accuracy of integrated PET-CT compared with dedicated PET alone for the staging of patients with nonsmall cell lung cancer. *Ann Thorac Surg* 2004; 78: 1017-1023.

38. Mitsuhashi A, Okuma Y, Zenke Y, Hosomi Y. Prognostic affects of osteoclast inhibitors in extensive stage small cell lung cancer patients with bone metastases. *Mol Clin Oncol* 2018; 9: 561-565.

39. Halpern BS, Scheepers C, Weber WA, Crawford TL, Fueger BJ, Phelps ME, Czernin J. Presurgical staging of nonsmall cell lung cancer: positron emission tomography, integrated positron emission tomography/CT, and software image fusion. *Chest* 2005; 128: 2289-2297.

40. Nakamoto Y, Senda M, Okada T, Sakamoto S, Saga T, Higashi T, Togashi K. Software-based fusion of PET and CT images for suspected recurrent lung cancer. *Mol Imaging Biol* 2008; 10: 147-153.

41. Yu HH, Tsai YY, Hoffe SE. Overview of diagnosis and management of metastatic disease to bone. *Cancer Control* 2012; 19: 84-91.

42. Choi J, Raghavan M. Diagnostic imaging and image-guided therapy of skeletal metastases. *Cancer Control* 2012; 19: 102-112.

43. Raad RA, Lala S, Allen JC, Babb J, Mitchell CW, Franceschi AM, Yohay K, Friedman KP. Comparison of hybrid 18F-fluorodeoxyglucose positron emission tomography/magnetic resonance imaging and positron emission tomography/computed tomography for evaluation of peripheral nerve sheath tumors in patients with neurofibromatosis type 1. *World J Nucl Med* 2018; 17: 241-248.

44. Khan S, Son H. Spinal Metastasis Characterized on FDG PET/CT in Head and Neck Squamous Cell Carcinoma. *Clin Nucl Med* 2017; 42: 860-861.